Theory of the electronic structure of dilute nitride alloys: beyond the band-anti-crossing model

2004 J. Phys.: Condens. Matter 16 S3257

(http://iopscience.iop.org/0953-8984/16/31/019)

INSTITUTE OF PHYSICS PUBLISHING JOURNAL OF PHYSICS: CONDENSED MATTER

J. Phys.: Condens. Matter **16** (2004) S3257–S3276 PII: S0953-8984(04)77729-2

Theory of the electronic structure of dilute nitride alloys: beyond the band-anti-crossing model

E P O'Reilly[1], **A Lindsay**[1] **and S Fahy**[1,2]

[1] NMRC, University College, Lee Maltings, Prospect Row, Cork, Republic of Ireland
[2] Department of Physics, University College Cork, Republic of Ireland

Received 12 March 2004
Published 23 July 2004
Online at stacks.iop.org/JPhysCM/16/S3257
doi:10.1088/0953-8984/16/31/019

Abstract

We use an sp^3s^* tight-binding Hamiltonian to investigate the band-anti-crossing (BAC) model for dilute GaN_xAs_{1-x} alloys. The BAC model describes the strong band-gap bowing at low N composition x in terms of an interaction between the conduction band edge (E_-) and a higher-lying band of localized nitrogen resonant states (E_+). We demonstrate that the E_- level can be described very accurately by the BAC model, in which we treat the nitrogen levels explicitly using a linear combination of isolated nitrogen resonant states (LCINS). We also use the LCINS results to identify E_+ in the full tight-binding calculations, showing that at low N composition E_+ forms a sharp resonance in the conduction band Γ-related density of states, which broadens rapidly at higher N composition when the E_+ level rises in energy to become degenerate with the larger L-related density of states. We then turn to the conduction band dispersion, showing that the two-level BAC model must be modified to give a quantitative understanding of the dispersion. We demonstrate that the unexpectedly large electron effective mass values observed in some GaNAs samples are due to hybridization between the conduction band edge and nitrogen states close to the band edge. Finally we show that there is a fundamental connection between the strong composition-dependence of the conduction-band-edge energy and the n-type carrier scattering cross-section in $Ga(In)N_xAs_{1-x}$ alloys, imposing general limits on the carrier mobility, comparable to the highest measured mobility in such alloys.

1. Introduction

The semiconductor alloy gallium (indium) nitride arsenide has attracted considerable attention in recent years. When a small fraction of arsenic atoms in GaAs is replaced by nitrogen the energy gap initially decreases rapidly, at about 0.1 eV/% of N for $x < \sim 0.03$ [1], with the measured conduction band edge mass also showing unexpectedly large values [2–6].

This behaviour is markedly different to conventional semiconductors, and is of interest both from a fundamental perspective and also because of its significant potential device applications. The strong bowing opens the possibility of using GaInNAs to get optical emission on a GaAs substrate at the technologically important wavelengths of 1.3 and 1.55 μm, considerably expanding the capabilities of GaAs for optoelectronics [7–10].

Our understanding of conventional III–V alloys has been built up through a range of approaches. Much progress is based on the use and application of relatively simple models, such as effective mass theory and the envelope function method [11–13] to describe electronic states in quantum wells and heterostructures. These simple and well-established models are underpinned and informed by more detailed and fundamental theoretical calculations, as well as by comparison with a wide range of experimental data.

The issue we review here is the development of appropriate models to describe the electronic structure of dilute nitride alloys. Two complementary approaches have been taken to explain their extreme behaviour, one based on detailed band structure calculations [14–18], the other on an experimentally observed band-anti-crossing (BAC) effect [19]. The two approaches have been highly successful in describing the band edge energies, and their variation upon annealing [20, 21]. The BAC model has also been successfully applied to interpret photoreflectance measurements both of bulk and quantum well GaNAs samples, identifying a higher energy feature (E_+) observed in bulk samples [19, 22, 23], and also providing a consistent interpretation of quantum well excited state transition energies across a wide range of samples, and as a function of hydrostatic pressure [24, 25]. Despite the wide success of the BAC model, there has until recently been one significant set of experimental data which has remain unexplained, namely the observed composition dependence of the conduction band edge effective mass in Ga(In)NAs alloys. Both the BAC model and detailed calculations predict an enhancement of the conduction band edge mass compared to GaAs. The BAC model provides a good estimate of the measured mass at very low N compositions [6] ($x < 0.05\%$) and also in indium-containing samples [5], but significantly underestimates the mass in GaN_xAs_{1-x} for $x > 0.1\%$ [3–6]. The electron relative effective mass, m_e^*, has now been determined using a range of different techniques, with a consistent trend emerging of unexpectedly large relative mass values in GaN_xAs_{1-x}, such as $m_e^* = 0.13$, 0.12 and even 0.19 for $x = 0.1$ [6], 1.2 [4] and 2.0% [4]. These measured mass values provide a stringent test of any model describing the electronic structure of GaN_xAs_{1-x} and related alloys.

We review here that these mass values and several other previously unresolved aspects of the band structure of $Ga(In)N_xAs_{1-x}$ can be quantitatively understood by combining the insights and approach of the empirical BAC model with the detailed information available from band structure calculations. The approach we present gives results in excellent quantitative agreement with experiment, providing a clear understanding of the observed variations in m_e^*, and even predicting in several instances a non-monotonic variation of mass with pressure. Our results also show clearly why the higher energy feature labelled E_+ only emerges for $x > \sim 0.2\%$ in photoreflectance measurements of bulk GaN_xAs_{1-x} [22, 23]. They are also relevant to the recent direct observation of the conduction band dispersion in $GaN_{0.0008}As_{0.9992}$ quantum wells using magnetotunnelling spectroscopy [26], and provide further insight into the low mobility values generally observed in $Ga(In)N_xAs_{1-x}$ alloys [2, 27, 28].

It is well-established that when a single N atom replaces an As atom in GaAs, it forms a resonant defect level above the conduction band edge of GaAs [29, 30]. This defect level arises because of the large difference in electronegativity and atomic size between N and As [31–33]. A major breakthrough was achieved for dilute nitride alloys with the demonstration by Walukiewicz and co-workers (using hydrostatic pressure techniques [19]) that the reduction in energy gap in $Ga(In)N_xAs_{1-x}$ is due to a band anti-crossing (BAC) interaction between

the conduction band edge and higher-lying localized nitrogen resonant states. Experimental studies of ultra-dilute nitride alloys show a range of resonant defect levels above the conduction band edge due to the formation of N complexes. These include, e.g. that a gallium atom with two N neighbours gives a resonant defect level close to the low temperature conduction band edge of GaAs [23, 24, 30]. Similar states are found in empirical pseudopotential [16, 17] and tight-binding [34] studies of N complexes. Such calculations support many aspects of the band-anti-crossing model, but also provide additional insight into the role of disorder and nitrogen clustering in GaNAs alloys. We will show below that many of the previously unexplained features in the band structure of dilute nitride alloys can be understood by modifying the BAC model to explicitly include the effects of nitrogen clusters and interactions between neighbouring nitrogen atoms placed at random within the alloy.

The approach we take here is to first consider ordered GaNAs, reviewing the insights we have obtained using a carefully parameterized tight-binding method to describe the electronic structure [21, 35]. Using ordered structures, we derive explicitly a two-level BAC model in section 2 to describe the conduction band edge, showing that the concept of localized N resonant states can remain valid even up to $x \sim 0.25$.

We then turn to consider disorder effects, using the sp^3s^* tight-binding Hamiltonian. We investigate how the inevitable disorder in the N distribution in Ga(In)NAs modifies the BAC model and its predictions. We show in section 3 that even in a disordered alloy the band gap bowing and composition dependence of E_+ can still be described very accurately by the BAC model, but with the BAC now explicitly treating the random distribution of N resonant states [34]. We then extend the analysis in section 4, to show that the inclusion of disorder effects can give a quantitative understanding of the measured variation of effective mass with x in $Ga(In)N_xAs_{1-x}$, and of the behaviour of the E_+ level at very low N compositions ($x < \sim 0.2\%$) [36].

We switch direction in section 5, to consider in particular the consequences of the strong band gap bowing on electron mobility in dilute nitride semiconductors. We show a fundamental connection between the conduction-band-edge energy and the n-type carrier scattering cross-section in the ultra-dilute limit, imposing general limits on the carrier mobility in such alloys [28, 37]. Within an independent scattering approximation, the carrier mobility is estimated to be $\sim$1000 $cm^2\ V^{-1}s^{-1}$ for a N atomic concentration of 1%, comparable to the highest measured mobility in high-quality GaInNAs samples at these N concentrations, but higher than that found in many samples. We speculate that consideration of a continuous band of N cluster states, as introduced in sections 3 and 4, should further reduce the calculated mobility, to values in closer agreement with experiment.

Overall, we conclude that a clear understanding is emerging concerning the electronic structure of dilute nitride alloys. Significant progress has been made, both through the use of the BAC model and more detailed theoretical studies, giving a quantitative description of the electronic structure, and enabling predictive design and analysis of GaInNAs-based heterostructures and optoelectronic devices.

2. Nitrogen resonant states in ordered GaN_xAs_{1-x} structures

The BAC model explains the extreme band gap bowing observed in $In_yGa_{1-y}N_xAs_{1-x}$ in terms of an interaction between two levels, one at energy E_c associated with the extended conduction band edge (CBE) state ψ_{c0} of the InGaAs matrix, and the other at energy E_N associated with the localized N impurity states ψ_N, with the two states linked by a matrix element V_{Nc} describing the interaction between them [19]. The CBE energy of $Ga(In)N_xAs_{1-x}$, E_-, is then given by

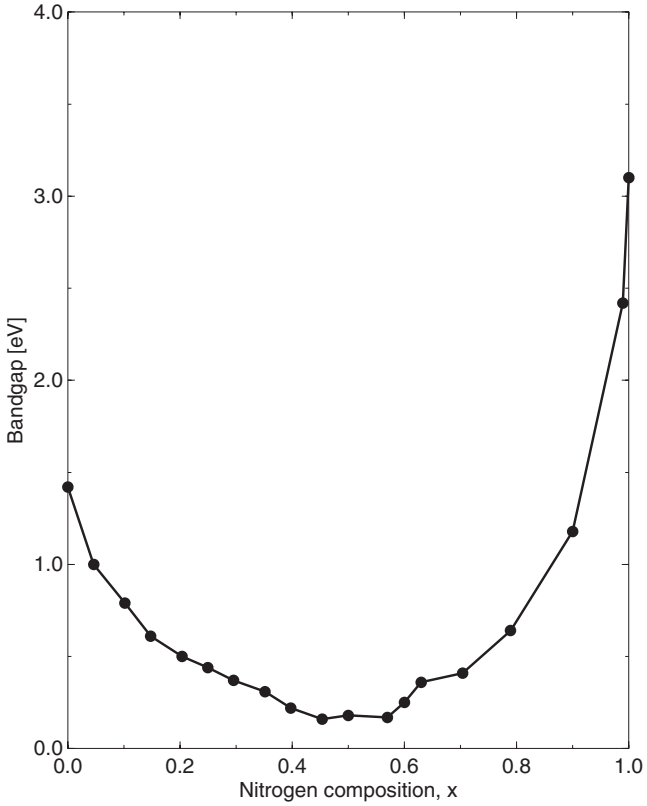

Figure 1. Variation of the band gap energy, E_g, in free-standing GaN_xAs_{1-x}, calculated across the full alloy range ($0 < x < 1$) using a carefully parameterized sp^3s^* Hamiltonian [21].

the lower eigenvalue of the determinant

$$\begin{vmatrix} E_N & V_{Nc} \\ V_{Nc} & E_c \end{vmatrix}. \tag{1}$$

A resonant feature associated with the upper eigenvalue, E_+, has also been observed in photoreflectance measurements [19, 22, 23], appearing in GaN_xAs_{1-x} for $x > \sim 0.2\%$ and remaining a relatively sharp feature until $x \sim 3\%$, beyond which composition it broadens and weakens, when the resonant state becomes degenerate with the L-related conduction band levels [34].

Although this two-level model provides a good description of the variation of E_- and E_+ with composition and annealing, it undoubtedly omits much of the detail of the band structure. Detailed calculations of large disordered clusters of GaN_xAs_{1-x} confirm the behaviour of E_-, while the E_+ state is also observed over a limited range of x [16, 17]. In addition, a series of N-related states are observed, with energies varying from close to the E_- level up towards E_+ [16]. These states are of secondary importance in understanding the band gap variation. We will show below when we introduce a modified form of the BAC model that they are key to understanding the observed variation of conduction band effective mass, and also of E_+.

To investigate the resonant state ψ_N, and its behaviour, we have developed an accurate sp^3s^* tight-binding (TB) Hamiltonian to describe the electronic structure of $GaInN_xAs_{1-x}$ [21]. This Hamiltonian fully accounts for the observed experimental data, and also gives results in good agreement with pseudopotential calculations [14, 16, 38, 39]. Figure 1 shows for instance

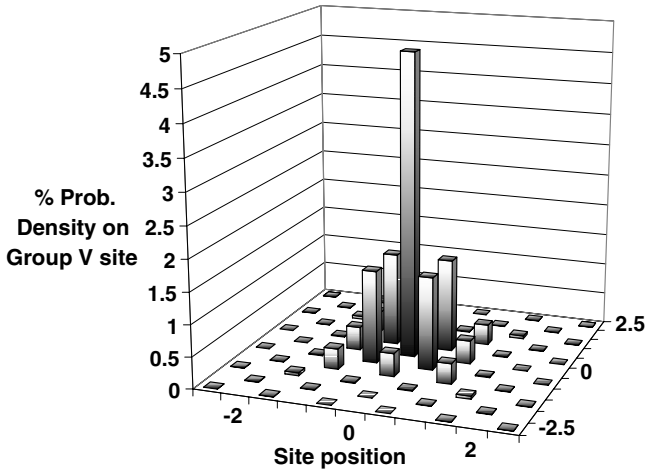

Figure 2. Calculated probability density of nitrogen resonant state, $|\psi_{N0}|^2$, projected onto the group V atoms in the (001) plane of a $Ga_{500}N_1As_{499}$ supercell, with the N atom situated in the centre of the plot, at (0, 0, 0), and the other group V atoms at lattice points $a(m/2, n/2, 0)$, $-5 \leqslant m, n \leqslant 5$.

the variation of the band gap energy across the full alloy range in free-standing GaN_xAs_{1-x}, calculated using the sp^3s^* Hamiltonian: the observed variation matches well that obtained in [38, 39].

To investigate the resonant state, and its behaviour, we calculated the electronic structure of ordered GaN_xAs_{1-x} supercells [21, 35]. By comparing the calculated CBE states ψ_{c1} and ψ_{c0} in large supercells ($Ga_{864}N_1As_{863}$ and $Ga_{864}As_{864}$, respectively), we can derive the nitrogen resonant state ψ_{N0} associated with an isolated N atom. In the BAC model, ψ_{c1} is a linear combination of ψ_{c0} and ψ_{N0}, with ψ_{N0} then given by

$$\psi_{N0} = \frac{\psi_{c1} - \alpha\psi_{c0}}{\sqrt{1-\alpha^2}} \tag{2}$$

where $\alpha = \langle\psi_{c1}|\psi_{c0}\rangle$. We find that ψ_{N0} is highly localized, with over 50% of its probability density on the N site and the four neighbouring Ga atoms (figure 2).

Because the N resonant state is so highly localized in figure 2, it is reasonable to expect that, as we increase the N density, we can associate a similar resonant level with each nitrogen site. To test if this is so, we compared the calculated resonant wavefunctions ψ_N for a series of increasingly smaller unit cells with the resonant state, $\psi_{N(0)}$, predicted by taking a linear combination of resonant wavefunctions from large unit cell calculations. We showed that to a very good approximation we can write the resonant wavefunction ψ_N at the zone centre as

$$\psi_N \approx \psi_{N(0)} = \frac{1}{\sqrt{\mathcal{N}}}\sum_{n=1}^{\mathcal{N}} \psi_{N0,n} \tag{3}$$

where ψ_N is represented by a linear combination of $\mathcal{N}$ isolated N states $\psi_{N0,n}$ located on an ordered array of sites $n = 1, \ldots, \mathcal{N}$ within the supercell. Figure 3(a) shows $|\langle\psi_N|\psi_{N(0)}\rangle|^2$, the modulus squared of the overlap between the predicted and calculated resonant states for simple cubic (sc, ◆) and face centred cubic (fcc, ●) nitrogen arrays. The overlap between the predicted and exact wavefunctions is almost unity, for $x < \sim 0.05$, and remains over 94% for the simple cubic structures, even up to $x = 0.25$ (a $Ga_4N_1As_3$ unit cell). This shows that the nature of the perturbation is indeed related to localized N states, even as far as $x = 0.25$, and, as a consequence, suggests we can use a similar representation to accurately describe

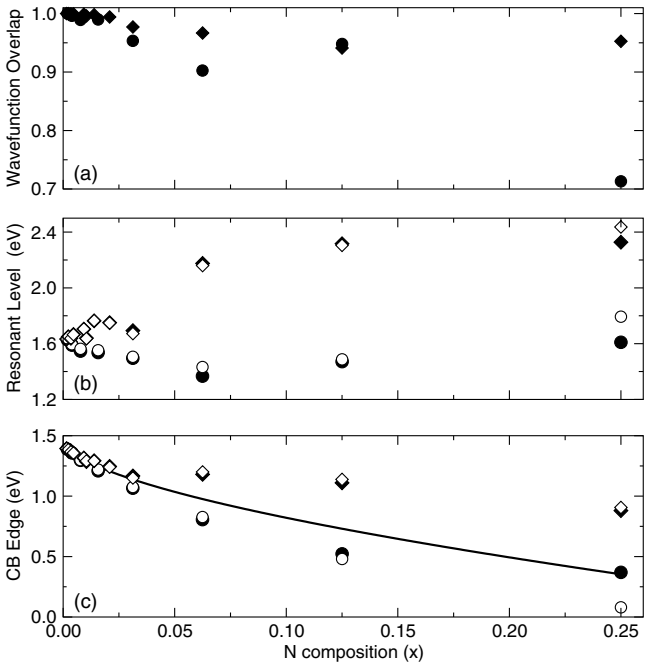

Figure 3. (a) Overlap between calculated and predicted resonant wavefunctions in simple cubic (◆) and face-centred cubic (●) supercells. (b) Resonant state energy, E_N, as a function of composition based on a full calculation (solid data points) and a simplified model (open data points). (c) Conduction band edge energy, E_c, of GaN_xAs_{1-x}, calculated using the full Hamiltonian (solid data points) and the two-band model of equation (1) (open data points).

the N-related states and conduction band edge in disordered GaN_xAs_{1-x} structures. We note that the overlap between the predicted and calculated resonant wavefunctions drops to ∼70% for the case of a $Ga_4N_1As_3$ 2 × 2 × 1 face-centred cubic structure [35]. This occurs because there is an infinite chain of nitrogen nearest neighbours in this structure. The symmetry is reduced about the N atoms in such a chain compared to isolated N states, due primarily to the unsymmetric nature of the lattice distortion parallel and perpendicular to the chain direction. This reduction in symmetry can significantly modify the resonant state wavefunction.

The filled data points in figure 3(b) show the calculated resonant energy, E_N, for each structure, found by evaluating $\langle\psi_N|H|\psi_N\rangle$ directly, while the filled data points in figure 3(c) show the calculated reduction in the conduction band edge energy as a function of N concentration in the ordered structures considered. The calculated values of E_N follow a non-monotonic trend, with the value of E_N generally being larger in the sc than in the fcc supercells considered, due to the directional dependence of the resonant state wavefunction [40] and of the perturbing potential, ΔV, introduced when an As atom is replaced by N.

The open data points in figure 3(b) show the value of E_N calculated for each structure by directly evaluating $\langle\psi_{N(0)}|H|\psi_{N(0)}\rangle$. These estimated values, $E_{N(0)}$, are in excellent agreement with the values of E_N obtained from the full calculation. Finally, the open data points in figure 3(c) were obtained by using the estimated values, $E_{N(0)}$ in equation (1), with E_c assumed to vary linearly and V_{Nc} explicitly calculated as $\langle\psi_{N(0)}|\Delta V|\psi_{c0}\rangle$. The very good agreement between the full calculation and this modified two-band model confirms the validity of the two-band model, although we see that the resonant state energy used, E_N, does depend on local environment, as discussed further below.

3. Influence of disorder on nitrogen resonant states, E_- and E_+ in GaN_xAs_{1-x}

Overall, figures 2 and 3 clearly demonstrate that the conduction band edge in GaN_xAs_{1-x} is being perturbed and pushed downwards due to its interaction with a higher-lying resonant state, centred on the nitrogen atoms. Why then has this state not been identified in previous calculations? To answer this question, and to investigate the role of disorder, we have extended the tight-binding and two-level model to disordered GaN_xAs_{1-x} supercells.

We first consider a set of 1000 atom supercells containing up to 15 randomly distributed N atoms. In these supercells we fit the number, but not the distribution, of N–N pairs to the number expected statistically, so that each cell contains n isolated N sites and p N–N pairs. For each configuration, we used the GULP molecular relaxation package [41] to calculate the equilibrium positions of all the atoms, using a parametrized valence force field (VFF) model, while using Végard's law to vary the unit cell basis vectors as $a(x) = xa_{GaN}+(1-x)a_{GaAs}$. The calculated relaxed bond lengths are in good agreement with those obtained by other authors [39] from *ab initio* pseudopotential calculations.

In a disordered supercell, we again expect the GaN_xAs_{1-x} conduction band edge to be formed as a linear combination of isolated nitrogen resonant states (LCINS) interacting with the unperturbed conduction band edge, ψ_{c0}. For the supercells considered here, we have n resonant basis states, $|\psi_{N0,i}\rangle$, associated with isolated N resonances ($i = 1-n$) and $2p$ resonant basis states associated with the p N–N pairs ($|\psi_{NN+,j}\rangle$ and $|\psi_{NN-,j}\rangle$, $j = 1-p$, which are even and odd, respectively, about the Ga site at the centre of the N–N pair). We write the sp^3s^* Hamiltonian H of the $Ga_{500}N_{n+2p}As_{500-n-2p}$ supercell as

$$H = H_0 + \Delta V_N + \Delta V_{NN} \tag{4}$$

where H_0 is the $Ga_{500}As_{500}$ Hamiltonian, ΔV_N the sum of defect potentials associated with the n isolated N atoms and ΔV_{NN} the sum of defect Hamiltonians associated with the p N–N pairs. In extension of the approach for ordered structures, we now determine the GaN_xAs_{1-x} conduction band edge E_- and the N-related conduction band levels by constructing and solving a $(n+2p+1)\times(n+2p+1)$ Hamiltonian matrix involving the GaAs conduction band edge wavefunction, $|\psi_{c0}\rangle$, and the $n+2p$ N-related states. We use the sp^3s^* Hamiltonian to evaluate explicitly each matrix element,

$$H_{\alpha\beta} = \langle\psi_\alpha|H|\psi_\beta\rangle \tag{5}$$

where α and $\beta = N0_i, \ldots, N0_n, NN+_j, \ldots, NN+_p, NN-_j, \ldots, NN-_p$ and c0. We also evaluate the overlap matrix, S, which has non-zero off-diagonal matrix elements $S_{\alpha\beta} = \langle\psi_\alpha|\psi_\beta\rangle$, due to the overlap between N resonant states centred on different sites within the supercell. The eigenvalues ε_α of the LCINS model are then obtained by solving the matrix equation

$$H\cdot u_\alpha = \varepsilon_\alpha S\cdot u_\alpha \tag{6}$$

with the eigenstates ϕ_α then given by

$$\phi_\alpha = \sum_i^n u^\alpha_{N0,i}\psi_{N0,i} + \sum_j^p (u^\alpha_{NN+,j}\psi_{NN+,j} + u^\alpha_{NN-,j}\psi_{NN-,j}) + u^\alpha_{c0}\psi_{c0}. \tag{7}$$

Figure 4 shows the results of the CBE energy and its Γ_{1c} character calculated using the full tight-binding (■) and LCINS (Δ) methods for five significantly different random structures of a 1000 atom $Ga_{500}N_mAs_{500-m}$ supercell containing (i) $m = 5$, (ii) $m = 10$ and (iii) $m = 15$ nitrogen atoms. The figures clearly show that both the CBE energy and its fractional Γ_{1c} character are given accurately by the LCINS model. Furthermore there is excellent correlation in the variation between different random structures. For example, in the supercell calculations

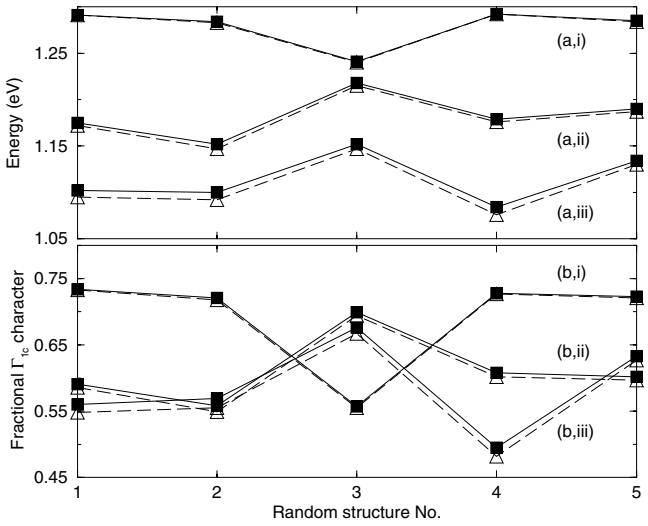

Figure 4. Variation in (a) the conduction band edge energy and (b) its fractional Γ_{1c} character between several different random $Ga_{500}N_m As_{500-m}$ supercell structures calculated using the full tight-binding (■) and LCINS (△) methods for (i) $m = 5$, (ii) $m = 10$ and (iii) $m = 15$.

containing $m = 15$ N atoms, the maximum variation in CBE energy between different random structures is ∼70 meV, while the maximum variation in CBE energy between the LCINS and full tight binding calculations is only ∼7 meV. This excellent correlation confirms the validity of describing the E_- state, and the band-gap bowing, as being due to an interaction between localized N resonant states and the host CBE.

We now turn to obtain a more detailed comparison between the higher-lying conduction states calculated using the LCINS and full tight-binding methods. There are again strong correlations between the two sets of results. The light vertical lines in figures 5(a) and (b) show the distribution of Γ_{1c} character across the conduction band spectrum of a $Ga_{500}N_{10}As_{490}$ supercell which includes one N–N pair, calculated using the full sp^3s^* tight-binding model. The inverted black lines in (a) show the weight of Γ_{1c} character on each of the eigenvalues E_α of the LCINS Hamiltonian of the same structure. The inverted black lines in (b) show the projection of the LCINS eigenstates φ_α, weighted by their Γ_{1c} character $|u^\alpha_{c0}|^2$, on to the conduction band states of the full sp^3s^* calculation.

A comparison of the results in figures 5(a) and (b) shows remarkable replication of the full Γ_{1c} spectrum by the LCINS model, demonstrating that even the more complex higher lying interacting states can be given accurately using isolated N and N–N pair states. Figure 5 is for a nitrogen concentration of $x = 2\%$.

For other structures considered, the agreement is also excellent, with even closer agreement at smaller x. A detailed analysis of figure 5 shows that the first 10 LCINS N-levels each correspond to a single sp^3s^* state below the energy of 1.75 eV: one at 1.21 eV (the E_- level) with a large Γ_{1c} component, one at 1.44 eV (the $E_{NN(+)}$ level) with a small Γ_{1c} component and eight closely spaced levels in the range 1.50–1.75 eV, which have a very weak admixture of Γ_{1c} character, and do not contribute to the band gap bowing. We see from figure 5(b, iii), in conjunction with the magnified inset region in figure 5(a), that these eight states project onto an equivalent eight levels in the full sp^3s^* calculations.

We identify the eleventh and highest-lying N state in figure 5, at 1.86 eV, with the E_+ level. It has the greatest interaction with the host-matrix conduction band edge state, with

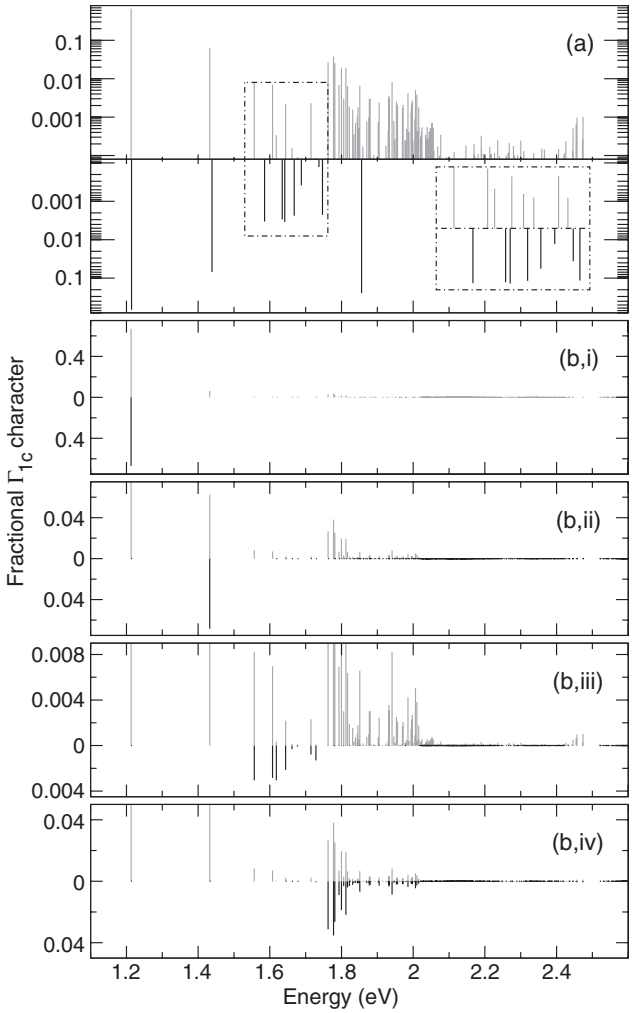

Figure 5. (a) GaAs Γ_{1c} character projected onto the conduction band states of a $Ga_{500}N_{10}As_{490}$ supercell for the full tight-binding (upper) and LCINS (lower) cases. (b) The lower lines are the projection of the (i) first, (ii) second, (iii) third–tenth and (iv) eleventh LCINS states onto the full tight-binding conduction band structure (upper, lighter lines).

$\sim$25% Γ_{1c} character, and projects on to a whole spectrum of sp^3s^* states with energy above 1.75 eV (figure 5(b, iv)). Because of the limited number of basis states in the LCINS model, it cannot replicate the width of a resonance, and the E_+ level is represented by a single state with energy close to the average energy of the resonance and Γ_{1c} character close to the integral sum across the width of the resonance.

In summary, analysing the eigenvectors of the LCINS calculation, it is straightforward to identify the different kinds of N state combinations, and the form of their interaction with the host conduction band edge (CBE). We can identify in figure 5(b) (i) the N-hybridized CBE, E_-, (ii) a low-lying group of states related to symmetric N–N pair states, E_2 (one of which is present in the supercell considered in figure 5), (iii) a complex combination of N states (including the anti-symmetric N–N pair state), which interact weakly with the CBE and which lie close to the isolated N state level, and (iv) a symmetric combination of states on all N atoms,

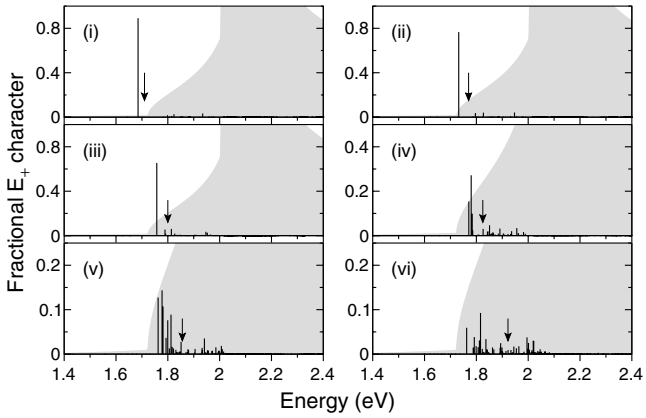

Figure 6. Projection of the LCINS E_+ level onto the conduction band states of disordered 1000-atom GaN_xAs_{1-x} supercells, with (i) $x = 0.4\%$, (ii) $x = 0.8\%$, (iii) $x = 1.0\%$, (iv) $x = 1.4\%$, (v) $x = 2.0\%$ and (vi) $x = 3.0\%$, showing the broadening of the E_+ resonance in the L-related GaAs density of states (shown on a similar scale in (eV atom)$^{-1}$). The arrow indicates the position of the LCINS E_+ level.

which appears as a resonance and which interacts strongly with the CBE. We have identified this last state as the E_+ level.

The E_+ state was observed in photoreflectance measurements [22, 23], appearing in GaN_xAs_{1-x} for $x > \sim 0.2\%$ and remaining a relatively sharp feature until $x \sim 3\%$, beyond which composition it broadens and weakens. The E_+ state was also observed at low N concentrations in pseudopotential calculations, but proved difficult to track to higher compositions [17]. Using the LCINS model, we identify here why E_+ is difficult to observe at higher compositions, by explicitly projecting the LCINS E_+ eigenvector φ_+ onto the eigenstates of a series of full sp^3s^* calculations. We will further consider the low composition case ($x \sim 0.2\%$) in the next section. Figure 6 shows the evolution of the E_+ state as given by the full sp^3s^* Hamiltonian and highlighted using LCINS for a series of 1000 atom supercell structures containing (i) 0.4%, (ii) 0.8%, (iii) 1%, (iv) 1.4%, (v) 2% and (vi) 3% of randomly distributed N atoms. Figures 6(i–iv) show E_+ as a very strongly highlighted feature, with a long, quickly decaying tail over higher energy states. In figures 6(v) and (vi) the E_+ state begins to break-up and spread out significantly. This change in the nature of E_+ is consistent with experiment, which shows a relatively strong feature at E_+ for $x \sim 1\%$ and which then becomes weaker and broader with increasing x up to $\sim$3% where it is hardly distinguishable at all [22]. We note that the strength of the resonance peak at larger x depends on where E_+ lies in the density of states of the host system, forming a sharp resonance in the conduction band Γ-related density of states, which broadens rapidly at higher N composition when the E_+ energy becomes degenerate with the larger L-related density of states.

Overall, we conclude from our detailed analysis of the full band structure calculations that the conduction band edge in GaN_xAs_{1-x} is indeed being perturbed and pushed downwards due to its interaction with a higher-lying band of localized nitrogen resonant states. We now turn to consider the effects of this band of localized nitrogen states on the conduction band dispersion and, in particular, on the band edge effective mass.

4. Conduction band structure and effective mass in disordered GaN_xAs_{1-x}

We can gain further insight into the band structure of a disordered $Ga_NN_MAs_{N-M}$ supercell by first diagonalizing the $M \times M$ matrix linking the individual N states, $|\psi_\alpha\rangle$, to get M

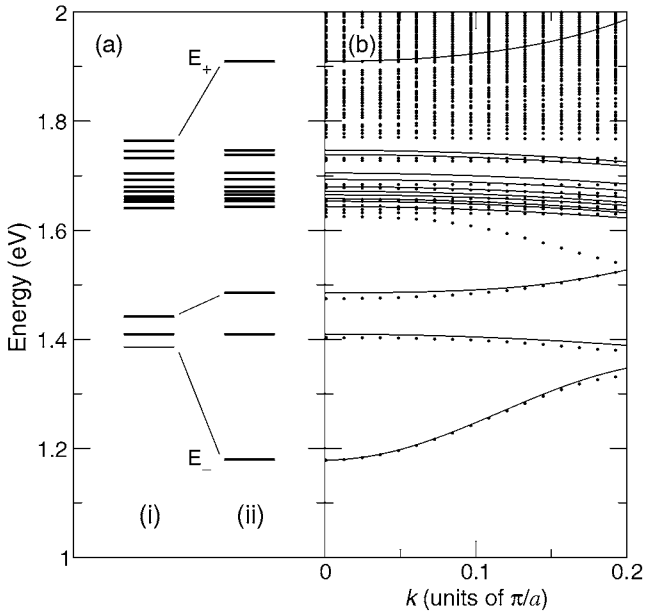

Figure 7. (a) Calculated N cluster state energies ε_l and CBE energy in a $Ga_{500}N_{13}As_{487}$ supercell (i) before and (ii) after inclusion of interaction with CBE; (b) supercell band dispersion calculated using tight-binding (dots) and LCINS method (solid curves).

nitrogen cluster states, ϕ_{Nl} with energy ε_l and then evaluating the interactions between the set of cluster states ϕ_{Nl} and the CBE, ψ_{c0}. Figure 7(a) shows (i) the N state energies ε_l and the CBE self-energy $\langle\psi_{c0}|H|\psi_{c0}\rangle$ (thin line) of an exemplar $Ga_{500}N_{13}As_{487}$ disordered supercell ($x = 2.6\%$; 2N–N pairs included), and (ii) the calculated zone-centre eigenvalues due to interactions between these cluster states and the unperturbed CBE state, ψ_{c0}. The dots in figure 7(b) show the band dispersion along the z-direction of this supercell, calculated using the full tight-binding method. As was the case in figure 5, very good agreement is obtained at the zone centre between the full calculations and the LCINS results, further confirming that the LCINS method describes well both the CB edge and the series of N-related states which lie above the CB edge.

The solid curves in figure 7(b) show the LCINS conduction band dispersion away from the zone centre, calculated using a $\mathbf{k}\cdot\mathbf{p}$ model which includes the standard Kane matrix element linking the valence band maximum with the unperturbed CBE state, ψ_{c0} [21, 42]. The close agreement between the LCINS $\mathbf{k}\cdot\mathbf{p}$ and the full tight-binding calculations for the lowest conduction bands confirms the validity of describing these states in terms of interactions between localized (but interacting) N resonant states and the unperturbed host matrix conduction band edge.

Because N introduces such a strong perturbation, the results of an individual calculation such as that in figure 5 or 7 depend strongly on the statistical distribution of the N atoms, including, e.g. the number of N–N pairs in the cluster, and the presence or otherwise of larger and less common N clusters. How then can we probe the average conduction band properties of randomly disordered GaN_xAs_{1-x} alloys? Figures 3, 5 and 7 each demonstrate the importance of the nitrogen cluster state energies ε_l, and the strength of their interactions $V_l = \langle\phi_{Nl}|H|\psi_{c0}\rangle$ with the CBE. We therefore investigate key aspects of the CB electronic

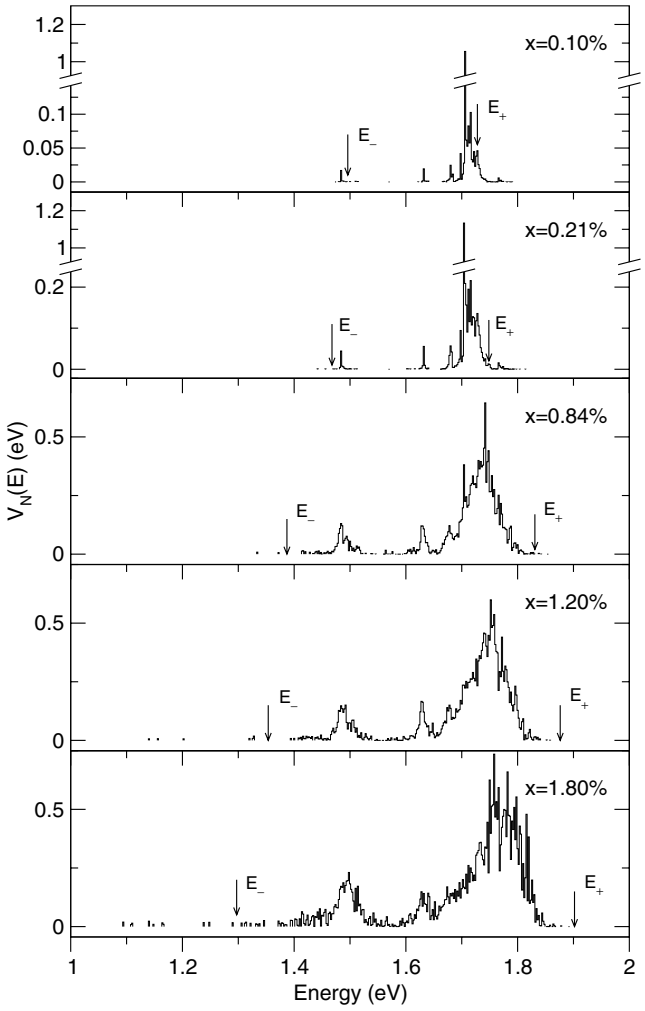

Figure 8. Calculated distribution of N cluster state energies, ε_l, weighted by their interactions, $|V_l|$ with the conduction band edge state for five bulk GaN_xAs_{1-x} compositions, with $x = 0.1\%$, 0.21%, 0.84%, 1.20% and 1.80%, respectively.

structure by placing $M = 8000$–$10\,000$ N atoms at random in an ultra-large GaN_xAs_{1-x} supercell, with the composition x determined by the size of the supercell considered. The large values of M are chosen to ensure minimal statistical variation between different random supercells.

The histograms in figure 8 show the distribution of the N state energies ε_l, and their interaction with the CBE state ψ_{c0} for $x = 0.1\%$, 0.2%, 0.84%, 1.2% and 1.8%, respectively, where we plot in each case

$$V_N(E) = \sum |V_l|^2 T(E - \varepsilon_l), \tag{8}$$

where $T(x)$ is a top-hat function of width 2 meV and unit area. It can be seen that for very low N composition ($x \leqslant \sim 0.2\%$), most of the interaction arises from states which lie close to the isolated N resonant level energy ($E_N = 1.666$ eV at 300 K; 1.706 eV at 0 K in our calculations). A small feature due to N–N pairs is observed about 1.446 eV at 300 K (1.486 eV at 0 K), with

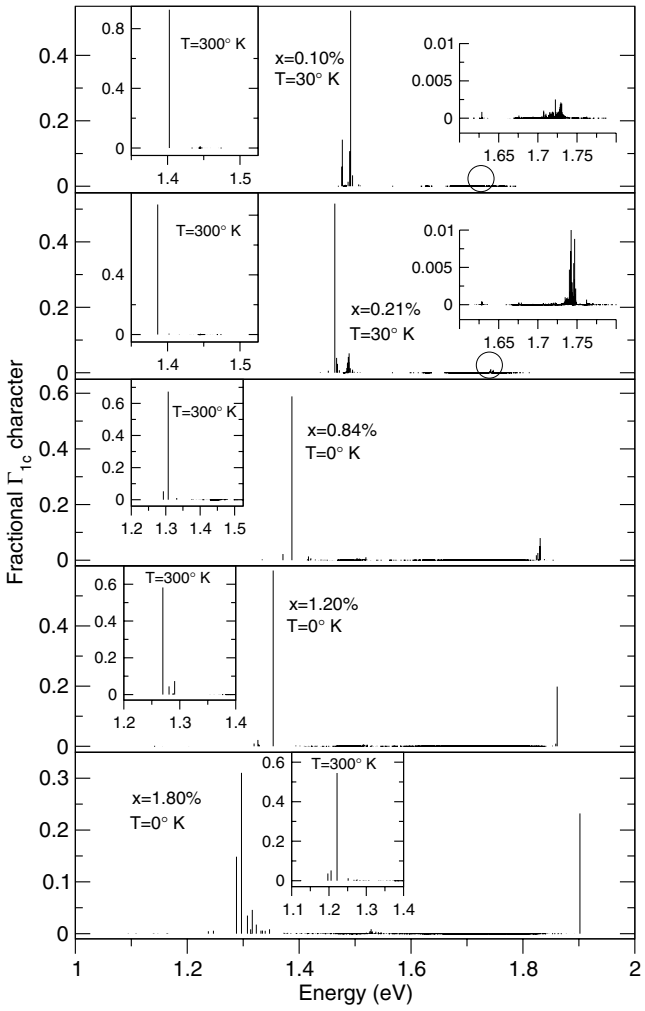

Figure 9. Calculated LCINS spectrum projected onto the unperturbed conduction band edge wavefunction ψ_{c0} for five bulk GaN_xAs_{1-x} compositions, with $x = 0.1\%$, 0.21%, 0.84%, 1.20% and 1.80%, respectively.

another weak feature at 1.594 eV at 300 K (1.634 eV at 0 K), due to second-neighbour N atoms on opposite corners of a cubic unit cell face. The energy spectrum of the N cluster states broadens considerably at higher N compositions, and a small number of isolated N states start to be observed below the N–N pair states, due to the random formation of a small proportion of larger N clusters in the supercell.

Extending the BAC model to these ultra-large supercells, we now calculate the effects of the interaction between these bands of N-related states and the unperturbed CBE wavefunction, ψ_{c0}, diagonalizing the $(M+1)\times(M+1)$ matrix linking ψ_{c0} with the M N-related levels. Figure 9 shows the calculated LCINS spectrum projected onto the unperturbed CBE wavefunction,

$$G_\Gamma(E) = \sum |a_{\Gamma i}|^2 T_2(E - E_i), \tag{9}$$

where $a_{\Gamma i}$ is the amplitude of the ith eigenstate, of energy E_i, on ψ_{c0}, and $T_2(x)$ is a narrow top-hat function of unit height. The results in figure 9 and related calculations are in excellent

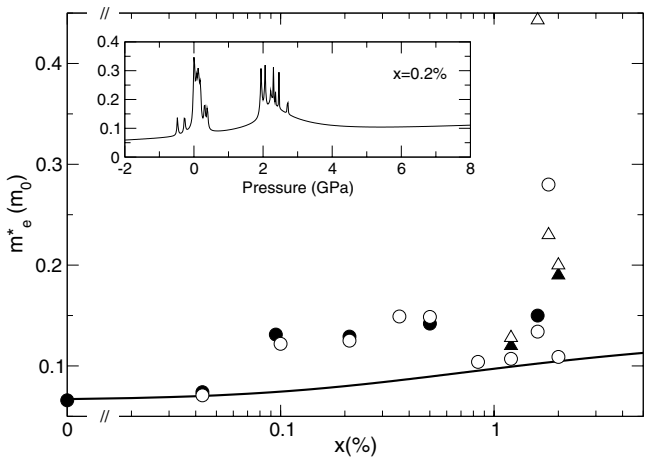

Figure 10. Solid data points: measured low temperature electron effective mass m_e^* in bulk (circles) and QW (triangles) samples. Open symbols (solid curve): m_e^* calculated using LCINS (BAC) method. Inset: calculated variation of m_e^* with pressure in a bulk $GaN_{0.0021}As_{0.9979}$ epilayer at $T = 0$ K.

agreement both with the BAC model and with experiment. Firstly, the interaction between the N resonant states and the CBE pushes the band edge downwards in energy. We find that the conduction band edge (defined as the low energy state with greatest Γ character) passes through the N–N pair states between $x = 0.1\%$ and 0.2% at $T = 0$ K, consistent with experiment [23]. The CBE shifts further down in energy relative to the N–N pair states at 300 K. Secondly, we observe the emergence of the E_+ level, with a single state with significant Γ character observed at higher energies for $x > \sim 0.2\%$. The E_+ level is not observed in GaN_xAs_{1-x} samples with $x \leqslant 0.1\%$. We see from figure 9 that this is due to the width of the band of N-related resonant states even at such low N compositions: the E_+ state from the BAC model is degenerate and thus hybridizes with this relatively wide N-related band, and so is not observed experimentally until higher nitrogen compositions.

One key feature of figure 9 is contrary to the two-level BAC model. When the CBE and N band interact with each other in equation (1), the fractional Γ character, $f_{\Gamma c}$, of the lower eigenvalue, E_-, must always exceed 50% ($f_{\Gamma c} > 0.5$). We see in figure 9, e.g. for $x = 0.2\%$, that $f_{\Gamma c} = 0.52$ at 0 K (0.87 at 300 K), while $f_{\Gamma c} = 0.32$ (0.54) at 0 K (300 K) for $x = 1.8\%$. The reduced values of $f_{\Gamma c}$ occur when E_- is close in energy with N–N pairs or other cluster states. Because of this accidental (near-)degeneracy, E_- hybridizes with these N-related states, thus leading to the reduced $f_{\Gamma c}$ value.

In the $\mathbf{k} \cdot \mathbf{p}$ model of figure 7, the conduction band edge effective mass is approximately proportional to the energy gap, and inversely proportional to $f_{\Gamma c}$ and the valence band fractional Γ character, $f_{\Gamma v}$. The filled circles (triangles) in figure 10 show the low temperature electron effective mass determined by a range of experimental techniques in bulk (quantum well) GaN_xAs_{1-x} samples [3–6]. The solid curve shows the predicted variation of the band edge effective mass in bulk GaN_xAs_{1-x} using the two-level BAC model of equation (1) [43]. This model significantly underestimates the measured mass even for x as low as 0.1%. The open symbols show the low temperature mass calculated for selected compositions, x, using the LCINS model, where we assume that

$$m_e^* = m_{e0}^* \frac{E_g(x)}{E_{g0} f_{\Gamma c} f_{\Gamma v}} \tag{10}$$

with $m^*_{e0} = 0.0667$ and $E_{g0} = 1.512$ eV for GaAs. $E_g(x)$ is the LCINS calculated energy gap, and $f_{\Gamma v}$ is taken to vary as $1 - x$ [44].

The calculated and experimental data are in remarkable agreement with each other, confirming that hybridization between the CB edge and nitrogen cluster states causes the observed enhancement of effective mass values. The density of N cluster states close to E_- varies both with composition x and with hydrostatic pressure p at a fixed composition in $Ga_{1-y}In_yN_xAs_{1-x}$. The inset in figure 10 shows the predicted variation of m^*_e with hydrostatic pressure, p, at $T = 0$ K in a $GaN_{0.002}As_{0.998}$ bulk epilayer. The mass m^*_e will initially increase with pressure, as the band edge passes through the N–N pair states, and should then drop rapidly with pressure towards the BAC value in the range of 0.5–1.5 GPa, before again increasing as hybridization with higher-lying N states occurs about 2 GPa. We also include negative pressure (to −2 GPa) in the inset. Although this cannot be achieved directly, a similar effect can be achieved by adding indium, because the CBE moves down relative to the nitrogen states with increasing y in $Ga_{1-y}In_yN_xAs_{1-x}$, thus accounting for the BAC-like masses observed in GaInNAs samples [5]. The application of hydrostatic pressure to GaInNAs should cause a significant increase in m^*_e, as the CBE passes through the lowest N-related levels. We note also from figure 10 that there can be a very low density of N cluster states close to E_- at moderate N composition (e.g. $x \sim 0.8\%$), giving a value of m^*_e close to the BAC value in such samples.

We see from figure 10 that a near-degeneracy with N cluster states significantly changes the band dispersion at the conduction band minimum. How will higher energy N states affect the conduction band dispersion? To address this issue, we have used a modified $\mathbf{k} \cdot \mathbf{p}$ model to calculate the conduction band dispersion for a series of bulk GaN_xAs_{1-x} structures, adding a valence band state $|\psi_{v0}\rangle$ to the LCINS model of section 3, and including a k-dependent Kane matrix element, kP, linking $|\psi_{v0}\rangle$ to the LCINS host matrix conduction band state $|\psi_{c0}\rangle$. Figure 11 shows the conduction band dispersion calculated for bulk GaN_xAs_{1-x} with (a) $x = 0.2\%$, (b) $x = 0.84\%$ and (c) $x = 1.8\%$, respectively. The dispersion is presented both for (i) $T = 0$ K and (ii) $T = 300$ K. The thick data points show LCINS states with $>10\%$ Γ_{1c} character; the thin data points are for 0.5–10% Γ_{1c} character, while the grey shading indicates states with 0.1–0.5% Γ_{1c} character. The zero of energy is taken relative to the GaAs valence band maximum.

The inclusion of N cluster states modifies the calculated band dispersion compared to that expected using the two-level BAC model of equation (1). At very low N compositions ((a), $x = 0.2\%$), two anti-crossing features are found in the lowest conduction band, one near the band minimum due to interactions with N–N pairs, and a second at about 1.6 eV, due to N–N second neighbours. With increasing N composition, the anti-crossing with the N–N pair states becomes more pronounced and the concept of a band dispersion starts to break down at larger k values (e.g. for (c) $x = 1.8\%$, $k > \sim\pi/a$, $E > 1.4$ eV).

The BAC model has been widely applied to investigate the conduction band dispersion in Ga(In)NAs, being used, e.g., both to analyse the gain characteristics of GaInNAs/GaAs quantum well laser devices [45–47], and also to interpret excited state transition energies in Ga(In)NAs quantum well structures [24, 25]. Although figure 11 shows that the BAC model can break down at higher energies, we conclude that it is still generally valid for such applications, particularly at room temperature. First, comparing (i) and (ii), we see that the breakdown of band dispersion in GaN_xAs_{1-x} occurs further from the band edge at 300 K than at 0 K, because of the difference in relative temperature dependence of the nitrogen state and conduction band edge energy [23, 48]. Second, previous calculations have shown that replacing gallium by indium in GaInNAs shifts the host conduction band edge downwards, and also pushes the energy of the N cluster states upwards relative to the cluster state energies in GaNAs.

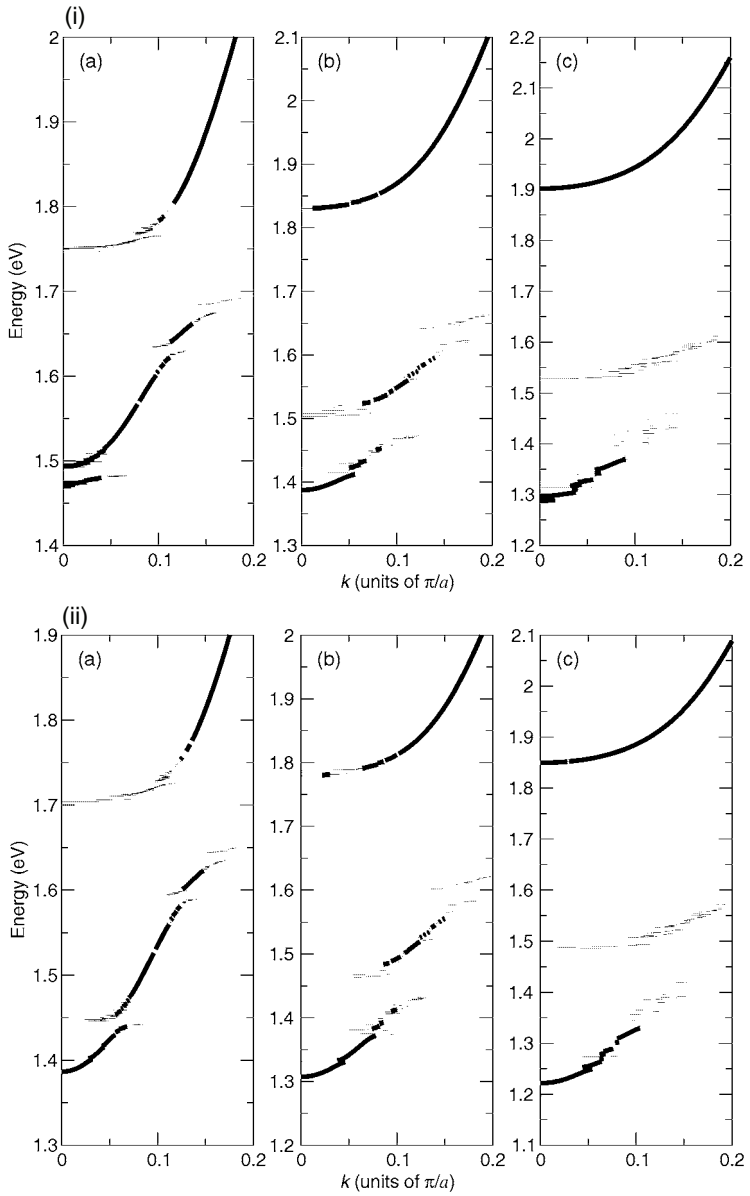

Figure 11. Conduction band dispersion calculated for bulk GaN_xAs_{1-x} using the LCINS method, with (a) $x = 0.2\%$, (b) $x = 0.84\%$ and (c) $x = 1.8\%$, respectively. The dispersion is presented both for (i) $T = 0$ K and (ii) $T = 300$ K.

We conclude therefore that the range of applicability of the two-level BAC model increases both with temperature and with indium content. Nevertheless, it may now be worthwhile re-considering the interpretation of some previous photoreflectance measurements, particularly where unexpected features were observed in the spectra [49], to see if some of these features might be due to band anti-crossing with lower-lying N-related defect levels.

5. Alloy scattering and mobility in dilute nitride alloys

There has until recently been little progress in developing models to describe the transport and mobility properties of dilute nitride alloys. Even for idealized random alloy crystals, these properties are difficult to analyse precisely because N introduces such a strong perturbation to the band structure of Ga(In)As. This must lead to strong alloy scattering. There is a well-established model [50], based on the Born approximation, to describe the relatively weak alloy scattering which occurs in conventional semiconductor alloys. This model is, however, entirely insufficient for extreme alloys such as GaNAs, underestimating the alloy scattering cross-section by over two orders of magnitude [28, 37]. We describe below how the strong scattering due to N atoms substantially limits the electron mobility in dilute nitride alloys, consistent with the maximum mobility observed experimentally of the order of 1000 $\mathrm{cm}^2\ \mathrm{V}^{-1}\mathrm{s}^{-1}$ [51].

We have calculated the scattering cross-section for an isolated N impurity in GaAs using *S*-matrix theory (distorted Born wave approach). This was previously applied to successfully describe resonant scattering due to conventional impurities in GaAs [52, 53]. For a sufficiently localized perturbation, ΔV_{N}, the total scattering cross-section σ for an isolated impurity is given by

$$\sigma = 4\pi \left(\frac{m^*}{2\pi\hbar^2}\right)^2 |\langle\psi_{\mathrm{c}1}|\Delta V_{\mathrm{N}}|\psi_{\mathrm{c}0}\rangle|^2\Omega^2, \tag{11}$$

where m^* is the electron effective mass at the band edge and Ω is the volume of the region in which the wavefunctions are normalized. The state $\psi_{\mathrm{c}0}$ is the Γ-point conduction band Bloch wavefunction (in the absence of the N atom) and $\psi_{\mathrm{c}1}$ is the exact band-edge state in the presence of the N atom.

We note that the Born approximation is equivalent to setting $\psi_{\mathrm{c}1} = \psi_{\mathrm{c}0}$ in the required matrix elements. It is often used in the discussion of conventional alloy and impurity scattering [50], but is entirely inadequate for the case of N defect scattering in GaAs.

Consider a perfect crystal for which the electron Hamiltonian is H_0 and the conduction band edge state has wavefunction $\psi_{\mathrm{c}0}$ and energy $E_{\mathrm{c}0}$. When we introduce a single N atom into a large volume Ω of the otherwise perfect lattice, the new Hamiltonian, $H_1 = H_0 + \Delta V_{\mathrm{N}}$, leads to a modified band edge state $\psi_{\mathrm{c}1}$ with energy $E_{\mathrm{c}1}$. We can therefore re-write the scattering matrix element as

$$\langle\psi_{\mathrm{c}1}|\Delta V_{\mathrm{N}}|\psi_{\mathrm{c}0}\rangle = \langle\psi_{\mathrm{c}1}|H_1 - H_0|\psi_{\mathrm{c}0}\rangle = (E_{\mathrm{c}1} - E_{\mathrm{c}0})\langle\psi_{\mathrm{c}1}|\psi_{\mathrm{c}0}\rangle. \tag{12}$$

Because $\langle\psi_{\mathrm{c}1}|\psi_{\mathrm{c}0}\rangle \to 1$ for sufficiently large Ω, we derive that at low impurity concentrations

$$\Omega\langle\psi_{\mathrm{c}1}|\Delta V_{\mathrm{N}}|\psi_{\mathrm{c}0}\rangle = \frac{\mathrm{d}E_{\mathrm{c}}}{\mathrm{d}n}, \tag{13}$$

where E_{c} is the conduction band edge energy and n is the number of impurities per unit volume. Substituting equation (13) in equation (11), and noting that n is related to the concentration x by $n = 4x/a_0^3$, where a_0 is the GaAs unit cell dimension, the scattering cross-section for an isolated impurity is then given by

$$\sigma = \frac{\pi}{4}\left(\frac{m^*}{2\pi\hbar^2}\right)^2 \left[\frac{\mathrm{d}E_{\mathrm{c}}}{\mathrm{d}x}\right]^2 a_0^6. \tag{14}$$

This result is key: it establishes a fundamental connection between the composition-dependence of the conduction-band-edge energy and the n-type carrier scattering cross-section in the ultra-dilute limit for semiconductor alloys, imposing general limits on the carrier mobility in such alloys.

We can see this by extending the isolated N result of equation (14) to the case of a dilute nitride alloy, $\mathrm{GaN}_x\mathrm{As}_{1-x}$. The mean-free path l of carriers depends in an independent

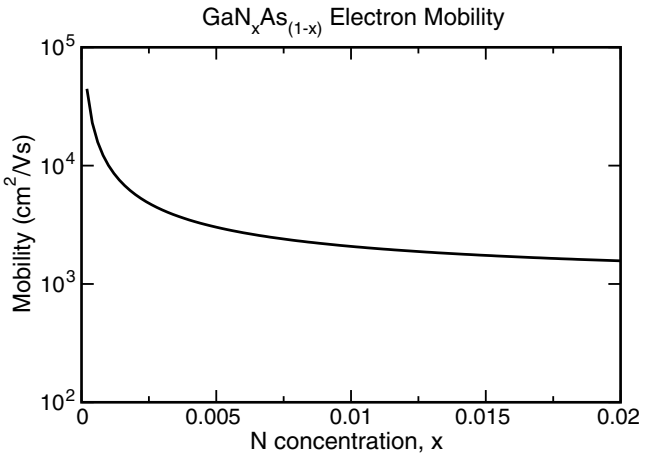

Figure 12. Room temperature variation of alloy-scattering limited electron mobility, μ, in GaN_xAs_{1-x}, calculated using equation (15).

scattering model on the scattering cross-section σ for a single defect and the number of defects n per unit volume as $l^{-1} = n\sigma$. Assuming such a classical model and the values of m^* and dE_c/dx at $x = 0$, we estimate for a N content of 1% a mean-free path of only 15 nm. This is still more than an order of magnitude larger than the average N separation, suggesting that an independent scattering model should remain appropriate in the dilute random alloy. The mobility μ is related to the mean-free path l as $\mu = e\tau/m^*$, with the scattering time $\tau = l/\bar{u}$, where $\bar{u}$ is the root mean square electron velocity. Setting $\bar{u}^2 = 3kT/m^*$, where T is the temperature, we estimate that the mobility μ is given by [28]

$$\mu^{-1} = \frac{\sqrt{3m^*kT}}{e}\pi\left(\frac{m^*}{2\pi\hbar^2}\right)^2\left[\frac{dE_c}{dx}\right]^2 a_0^3\, x. \tag{15}$$

Figure 12 shows the estimated variation of the room temperature electron mobility with x in GaN_xAs_{1-x}, calculated allowing both m^* and dE_c/dx to vary with x based on the two-level model of equation (1). The electron mobility is estimated to be of order 1000 cm^2 V^{-1}s^{-1} when $x = 1\%$, of similar magnitude to the highest values observed to date in dilute nitride alloys [51], but larger than that found in many samples, where $\mu \sim$ 100–400 cm^2 V^{-1}s^{-1} [2, 27, 54–57]. We note that factors omitted in the calculation here, including the influence of N–N nearest-neighbour pairs and clusters [16, 34], may contribute to limiting the mobility in actual samples [37]. In addition, film quality and composition fluctuations may also play a role in some samples. The intrinsic alloy-scattering-limited mobility should be larger in GaInNAs samples, due to the weaker band-gap bowing observed in indium-containing samples [24].

The intrinsically low electron mobilities in dilute nitride alloys have significant consequences for potential device applications. The low electron mobility, combined with the short non-radiative lifetimes observed to date, limit the electron diffusion lengths and efficiency achievable in GaInNAs-based solar cells. Further efforts may lead to increased non-radiative lifetimes, but are unlikely to see significant further improvements in the alloy-scattering limited mobility [51]. The low electron mobility generally observed to date may lead to reduced surface recombination in mesa structures containing GaInNAs quantum wells, of benefit for ultra-compact photonic device applications.

6. Conclusions

We demonstrate that the E_- level can be described very accurately by the BAC model, in which we treat the nitrogen levels explicitly using a linear combination of isolated nitrogen resonant states (LCINS). We also use the LCINS results to identify E_+ in the full tight-binding calculations, showing that at low N composition E_+ forms a sharp resonance in the conduction band Γ-related density of states, which broadens rapidly at higher N composition when the E_+ level rises in energy to become degenerate with the larger L-related density of states. We then turn to the conduction band dispersion, showing that the two-level BAC model must be modified to give a quantitative understanding of the dispersion. We demonstrate that the unexpectedly large electron effective mass values observed in some GaNAs samples are due to hybridization between the conduction band edge and nitrogen states close to the band edge. Finally we show that there is a fundamental connection between the strong composition-dependence of the conduction-band-edge energy and the n-type carrier scattering cross-section in $Ga(In)N_xAs_{1-x}$ alloys, imposing general limits on the carrier mobility, comparable to the highest measured mobility in such alloys.

Acknowledgments

We would like to thank many colleagues for useful discussions and collaboration on the electronic structure of GaInNAs. These include Alf Adams, Aleksey Andreev, Stelios Choulis, Robin Fehse, Joerg Hader, Jeff Hosea, Peter Klar, Stephan Koch, Henning Riechert, Stanko Tomić and Bernie Weinstein. We are grateful to Science Foundation Ireland for financial support.

References

[1] Weyers M, Sato M and Ando H 1992 *Japan. J. Appl. Phys.* **31** L853
[2] Skierbiszewski C 2002 *Semicond. Sci. Technol.* **17** 803
[3] Buyanova I A, Pozina G, Hai P N, Chen W M, Xin H P and Tu C W 2000 *Phys. Rev.* B **63** 033303
[4] Hai P N, Chen W M, Buyanova I A, Xin H P and Tu C W 2000 *Appl. Phys. Lett.* **77** 1843
[5] Baldassarri Höger von Högersthal G, Polimeni A, Masia F, Bissiri M, Capizzi M, Gollub D, Fischer M and Forchel A 2003 *Phys. Rev.* B **67** 233304
[6] Masia F, Polimeni A, Baldassarri Höger von Högersthal G, Bissiri M, Capizzi M, Klar P J and Stolz W 2003 *Appl. Phys. Lett.* **82** 4474
[7] Kondow M, Kitatani T, Larson M C, Nakahara K, Uomi K and Inoue H 1998 *J. Cryst. Growth* **188** 255
[8] Riechert H, Egorov A Y, Livshits D, Borchert B and Illek S 2000 *Nanotechnology* **11** 201
[9] Choquette K D *et al* 2002 *Electron. Lett.* **36** 1388
[10] Steinle G, Riechert H and Egorov A Y 2001 *Electron. Lett.* **37** 93
[11] Bastard G 1990 *Wave Mechanics Applied to Semiconductor Heterostructures* (Paris: Editions de Physique)
[12] Burt M G 1999 *J. Phys.: Condens. Matter* **11** R53
[13] Meney A T, Gonul B and O'Reilly E P 1994 *Phys. Rev.* B **50** 10893
[14] Mattila T, Wei S H and Zunger A 1999 *Phys. Rev.* B **60** R11245
[15] Jones E D, Modine N A, Allerman A A, Kurtz S R, Wright A F, Tozer S T and Wei X 1999 *Phys. Rev.* B **60** 4430
[16] Kent P R C and Zunger A 2001 *Phys. Rev.* B **64** 115208
[17] Kent P R C, Bellaiche L and Zunger A 2002 *Semicond. Sci. Technol.* **17** 851
[18] Kent P R C and Zunger A 2003 *Appl. Phys. Lett.* **82** 559
[19] Shan W, Walukiewicz W, Ager J W III, Haller E E, Geisz J F, Friedman D J, Olson J M and Kurtz S R 1999 *Phys. Rev. Lett.* **82** 1221
[20] Kim K and Zunger A 2001 *Phys. Rev. Lett.* **86** 2609
[21] O'Reilly E P, Lindsay A, Tomić S and Kamal-Saadi M 2002 *Semicond. Sci. Technol.* **17** 870

[22] Perkins J D, Mascarenhas A, Zhang Y, Geisz J F, Friedman D J, Olson J M and Kurtz S R 1999 *Phys. Rev. Lett.* **82** 3312
[23] Klar P J, Grüning H, Heimbrodt W, Koch J, Höhnsdorf F, Stolz W, Vicente P M A and Camassel J 2000 *Appl. Phys. Lett.* **76** 3439
[24] Klar P J *et al* 2002 *Semicond. Sci. Technol.* **17** 830
[25] Tomić S, O'Reilly E P, Klar P J, Grüning H, Heimbrodt W, Chen W M and Buyanova I A 2004 *Phys. Rev.* B at press
[26] Endicott J, Patanè A, Ibáñez J, Eaves L, Bissiri M, Hopkinson M, Airey R and Hill G 2003 *Phys. Rev. Lett.* **91** 126802
[27] Geisz J F and Friedman D J 2002 *Semicond. Sci. Technol.* **17** 769
[28] Fahy S and O'Reilly E P 2003 *Appl. Phys. Lett.* **83** 3731
[29] Wolford D J, Bradley J A, Fry K and Thompson J 1984 *Proc. 17th Int. Conf. on the Physics of Semiconductors* (New York: Springer)
[30] Liu X, Pistol M-E, Samuelson L, Schwetlick S and Seifert W 1990 *Appl. Phys. Lett.* **56** 1451
[31] Vogl P 1984 *Adv. Electron. Electron Phys.* **62** 101
[32] Hjalmarson H P, Vogl P, Wolford D J and Dow J D 1980 *Phys. Rev. Lett.* **44** 810
[33] Lindsay A and O'Reilly E P 2003 *Physica* B **340–342** 434
[34] Lindsay A and O'Reilly E P 2004 *Physica* E **21** 901
[35] Lindsay A and O'Reilly E P 2001 *Solid State Commun.* **118** 313
[36] Lindsay A and O'Reilly E P 2004 *Phys. Rev. Lett.* submitted
[37] Fahy S and O'Reilly E P 2004 *Physica* E **21** 881
[38] Bellaiche L, Wei S-H and Zunger A 1996 *Phys. Rev.* B **54** 17568
[39] Wei S-H and Zunger A 1996 *Phys. Rev. Lett.* **76** 664
[40] O'Reilly E P and Lindsay A 2000 *High Pressure Res.* **18** 13
[41] Gale J D 1997 *JCS Faraday Trans.* **93** 629
[42] O'Reilly E P and Lindsay A 1999 *Phys. Status Solidi* b **216** 131
[43] Wu J, Shan W, Walukiewicz W, Yu K M, Ager J W III, Haller E E, Xin H P and Tu C W 2001 *Phys. Rev.* B **64** 085320
[44] Lindsay A and O'Reilly E P 1999 *Solid State Commun.* **112** 443
[45] Hofmann M *et al* 2001 *Appl. Phys. Lett.* **78** 3009
[46] Hofmann M R *et al* 2002 *IEEE J. Quantum Electron.* **38** 213
[47] Tomić S, O'Reilly E P, Fehse R, Sweeney S J, Adams A R, Andreev A D, Choulis S A, Hosea T J C and Riechert H 2003 *IEEE J. Sel. Top. Quantum Electron.* **9** 1228
[48] Suemune I, Uesugi K and Walukiewicz W 2000 *Appl. Phys. Lett.* **77** 3021
[49] Klar P J, Grüning H, Koch J, Schäfer S, Volz K, Stolz W, Heimbrodt W, Kamal Saadi A M, Lindsay A and O'Reilly E P 2001 *Phys. Rev.* B **64** 121203(R)
[50] Harrison J and Hauser J R 1976 *Phys. Rev.* B **13** 5347
[51] Volz K, Koch J, Kunert B and Stolz W 2003 *J. Cryst. Growth* **248** 451
[52] Sankey O F, Dow J D and Hess K 1982 *Appl. Phys. Lett.* **41** 664
[53] Fisher M A, Adams A R, O'Reilly E P and Harris J J 1987 *Phys. Rev. Lett.* **59** 2341
[54] Geisz J F, Friedman D J, Olson J M, Kurtz S R and Keyes B M 1998 *J. Cryst. Growth* **195** 401
[55] Hong Y G, Tu C W and Ahrenkiel R K 2001 *J. Cryst. Growth* **227/228** 536
[56] Kurtz S R, Allerman A A, Seager C H, Sieg R M and Jones E D 2000 *Appl. Phys. Lett.* **77** 400
[57] Li W, Pessa M, Toivonen J and Lipsanen H 2001 *Phys. Rev.* B **64** 113308